Chapter 2

Modeling and Control of Wind Turbine to Damp the Power Oscillation

Emad M. Elhaji

Additional information is available at the end of the chapter

http://dx.doi.org/10.5772/intechopen.74835

Abstract

Damping inter-area oscillation by using a permanent magnet synchronous generator (PMSG) wind turbine is considered. The PMSG wind turbine is connected to the IEEE-30 bus power system at different buses. H-infinity design controller is proposed to modulate the power where the input of the H-infinity control is the variation of the local grid generator speed and the output is feedback to activate the PMSG speed control, blade pitch angle control and dc voltage control. MATLAB/SIMULINK is used in this study. The IEEE-30 bus system is reduced to 7 buses based on the number of generators to simplify the stability study. The method is applied to a seven-area power system that exhibits undamped oscillations. Results presented in this study demonstrate the effectiveness of the wind generator in increasing system damping considerably.

Keywords: permanent magnet synchronous generator, IEEE 30 bus system, reduced system, wind generator, H-infinity, inter-area oscillation, dynamic stability, small signal stability

1. Introduction

The reason to use the renewable energy is to reduce the pollution emissions such as carbon dioxide CO_2 in the air. Renewable energy such as wind energy is one of the cost-effective forms of energy available today to generate electricity [1, 2]. The development of modern wind energy started almost 30 years ago but were not installed significantly for long period. Over the past decade, the power from wind turbines increased from 23,900 to 486,790 MW from 2001 to 2016, respectively [3, 4]. The blade size of modern wind turbines has increased to increase the amount of power from the wind [4, 5]. In general, two types of wind turbine can be installed to the power grid such as fixed-speed wind turbine and variable-speed wind

turbine. The fixed speed wind turbines were installed in early 1990 to generate electricity regards of wind speed. This kind of wind turbines connected directly to the grid and its speed fixed at speed determined by the frequency of the grid [6–8]. After that in 1996, the variable speed wind turbine started connecting to the grid [9]. The classification of these turbines, fixed speed and variable speed wind turbines, is based on the principle of the generator and its operation [10]. The induction generator specifically squirrel cage induction generator is used with fixed speed wind turbine [11, 12]. In variable speed wind turbine two kind of generators can be used such as permanent magnet synchronous generator (PMSG) and doubly-fed induction generator (DFIG) [13–15]. Various of controls scheme can be applied in fixed and variable speed wind turbines such as stall control, blade pitch angle control, active stall control, dc voltage control, torque control and point of common coupling control (PCC) [16]. Nowadays, most of the wind turbines installed in power system are permanent magnet synchronous generator (PMSG) and doubly-fed induction generator (DFIG). PMSG connected directly to the power grid via back to back converter; therefore, the power from wind directly transferred to the grid. On the other hand, DFIG has two windings; stator winding connected directly to the power grid and rotor winding connected to the power grid via back to back converter [17, 18]. Therefore, the power from the wind transferees to the grid via stator and rotor. From the stator, the wind power directly transferees to the grid while from the rotor the power transferees to the grid or grid to the rotor depends on the operating conditions: over-synchronous condition if the power flows from rotor to grid and sub-synchronous condition if the power flows from grid to the rotor. DFIG required a slip rings to operate properly, but it has a high maintenance cost in long run for normal operation [13, 18].

The PMSG will be focused in this study. It is called also a brushless DC machine and just the rotor of the DC machine is replaced by a permanent magnet. Therefore, the PMSG will be a small in size compared to the DC machine, and the inertia of a PMSG will be higher. The result, PMSG has a good reliability and more higher power compared to the size [12, 14, 19]. In wind turbines application, the small generator in size with a higher power is preferred because the generator of wind turbine is placed hundreds of above the ground and then reduce the maintenance cost. The PMSG also has a back-to-back converter to control the flowing power from the wind, but it increases the cost of the PMSG in addition to the expensive permanent magnets [12, 14]. The maintenance of the PMSG is nearly free; therefore, it is highly desirable for wind turbine applications. Now, PMSG wind turbine is focused in area of research [12, 14].

When the wind turbines penetration to the power grid, the system stability become more significant. The PMSG is investigated for its capability to enhance the damping of dynamic oscillations in a multi-area system. The basic control applied to the PMSG is a field orientation control (FOC) [20, 21]. FOC is widely used in a research area especially in wind turbines. The FOC implemented in generator and grid sides of PMSG wind turbine to control the wind power that transferred to the grid [20, 21]. The synchronous frame of reference, a d-q frame of reference, is applied to the modeling of the generator side and grid side and a decoupled strategy is used to simplify the control design of the FOC. The proportional integral controls are used in the FOC in both sides of wind turbine as a result of a good steady state error. In generator side, the FOC is designed to control the torque of PMSG wind turbine by controlling the q-axis current of PM generator while in grid side, it is designed to control the dc voltage to

guarantee the power transfers from the wind to the grid. The FOC cannot damp any oscillation if there is any disturbance happen on the system such as wind speed change, power load change or symmetrical and unsymmetrical fault. These disturbances will cause a low-frequency oscillation due to many synchronous generators and wind turbines located in many areas with long tie-line as in **Figure 1** [22]. This oscillation with a range of frequency between 0.1 and 0.8 HZ is known as an inter-area oscillation [23, 24]. The system will be unstable if this oscillation increase in amplitude. Therefore, to make the system more stable, an auxiliary feedback control has to be added to damp the oscillation.

In [25–27], numerous of controls are applied to the PMSG wind turbine concern with the stability under the presence of grid dynamics. In [28, 29], implemented some devices to improve the system stability such as power system stabilizer (PSS) and flexible alternative current transmission system (FACTS), but these devices may not be sufficient to damp inter-are oscillations at high penetrations levels. In some literature use the frequency feedback in DFIG to damp the oscillation [30, 31]. In this study, the dynamic of the PMSG wind turbine is discussed through a suitable small-signal model. The PMSG connected to the IEEE 30 bus system at different buses such as generator and load buses. The PMSG wind turbine model is linearized and reduced in order to simplify the analysis of the system. This model is applied to case of damping the inter-area oscillation. To damp the inter-area oscillation, three modulation feedback loops were applied: dc-ink voltage, PMSG speed and blade pitch angle modulation. The feedback design method used in the study is based on the H-infinity control concept [32–35].

Section 2 describes a suitable dynamic model of the PM wind generator that can be used in dynamic studies. Section 3 demonstrates the small signal stability. Section 4 describes the H-infinity control method. Section 5 describes the simulation results and Section 5 provides the conclusion.

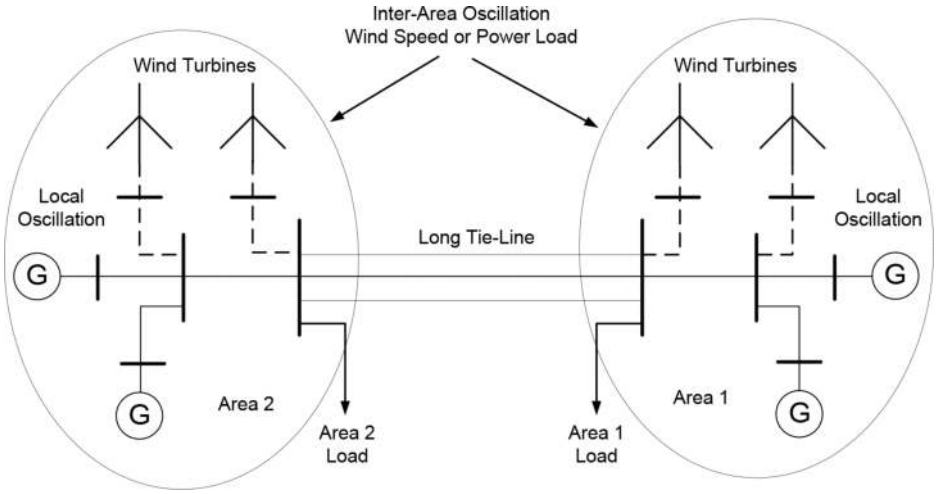

Figure 1. Two area power system connected with many of synchronous generators and wind turbines.

2. System modeling

The rotational of the wind turbine rotor blade converts the kinetic energy of the wind to the mechanical power. The mechanical power converts by the generator to the electrical power that is fed to the grid through a back-to-back converter. The wind turbine scheme as shown in **Figure 2** combines the mechanical subsystem and electrical subsystem. The mechanical subsystem includes the two mass system and rotor shaft, and the electrical subsystem includes a PMSG, back-to-back converter, and grid. The interconnection system modeling of the generator and grid sides are described in an appropriate frame for developing a suitable control scheme which will be discussed in detail in the following section [35–41]. The modeling of the both sides of wind turbine as well as back to back converter will be in details in the following section.

2.1. Wind turbine model

The extracted power from the wind turbine can be expressed as in (Eq. (1)) [13, 14, 19]; where σ is the air density, R is the blade radius, v_w is the wind speed, $C_p(\lambda,\beta)$ is the turbine power coefficient and it is a nonlinear function as in (Eq. (2)). The value coefficients in (Eq. (2)) c_1 to c_6 c_6 are: $c_1 = 0.5167$, $c_2 = 116$, $c_3 = 0.4$, $c_4 = 5$, $c_5 = 21$, and $c_6 = 0.0068$ [17]. Also, the torque of wind turbine can be presented in terms of the wind power and rotational speed of the shaft as in (Eq. (3)) [27, 37, 42–44].

$$P_w = \frac{1}{2}\,\sigma\,\pi R^2\,C_p(\lambda,\beta)v_w^3 \tag{1}$$

$$C_p(\lambda,\beta) = c_1\left(c_2\left(\frac{1}{\lambda-0.008\,\beta}-\frac{0.035}{\beta^3+1}\right)-c_3\,\beta-c_4\right)e^{-c_5\left(\frac{1}{\lambda-0.008\,\beta}-\frac{0.035}{\beta^3+1}\right)}+c_6\,\lambda,\qquad \lambda=\frac{R\,\omega_T}{v_w} \tag{2}$$

$$T_w = \frac{P_w}{\omega_T} = \frac{1}{2}\,\frac{\sigma\pi R^3}{\lambda}\,C_p(\lambda,\beta)v_w^2 \tag{3}$$

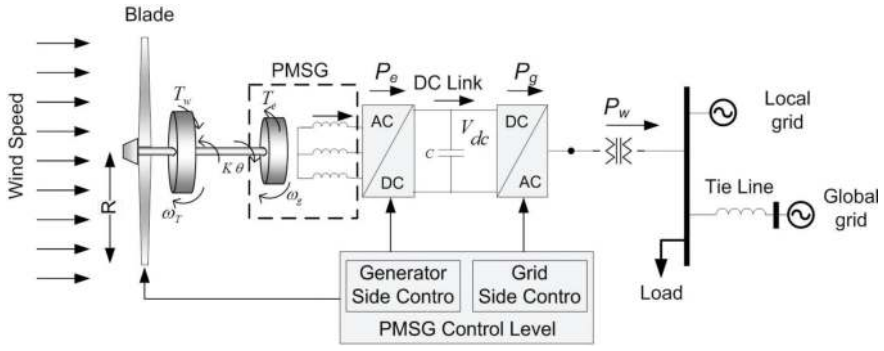

Figure 2. Configuration of the permanent magnet synchronous generator wind turbine.

Figure 3 shows the turbine power coefficient at different tip ratio and blade pitch angle. As seen from the same figure, the maximum value of power coefficient is 0.48 when the tip ratio is 8.1 and blade pitch angle is zero. The blade pitch angle control is zero that mean the wind speed is equal or less than the rated speed. The rated wind speed which extracted the maximum power is 12 m/s. The blade pitch angle control activates when the wind speed is more the rated value to decrease the turbine power coefficient so as to $C_p(\lambda, \beta)$ achieve the maximum power extracted from the wind.

2.2. Permanent magnet synchronous generator (PMSG) model

The dynamic model of the PMSG is derived based on the two-phase d-q synchronous frame of reference and **Figure 4** shows its equivalent circuit [27, 43, 44]. The electrical model of the PMSG in the synchronous frame of reference is by

$$\begin{aligned} v_{sd} &= -R_s i_{sd} - L_{sd}\frac{d\, i_{sd}}{dt} - \omega_e L_{sq} i_{sq} \\ v_{sq} &= -R_s i_{sq} - L_{sq}\frac{d\, i_{sq}}{dt} + \omega_e L_{sd} i_{sd} + \omega_e \psi_f \end{aligned} \tag{4}$$

where R_s is the armature resistance, $L_{ls}L_{sd}$, L_{sq} are the inductance in d-q axes and they are equal in the round rotor, ψ_f is the permanent magnetic flux, $\omega_e = p\,\omega_g$ is the electrical rotating speed, ω_g is related to the mechanical rotating speed of the generator, and p is the number of pole pairs.

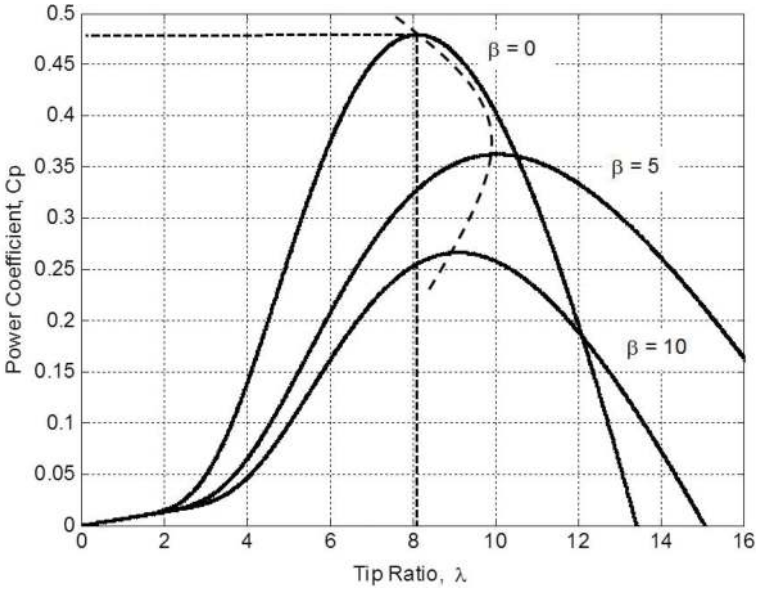

Figure 3. Power coefficient and tip ratio.

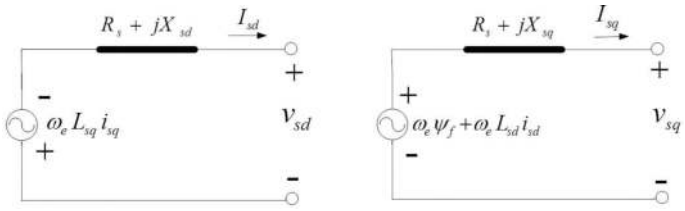

Figure 4. Equivalent circuit of PMSG.

The expressions of the electromagnetic torque T_e and active power of the PMSG P_e are given by [27, 44].

$$T_e = \frac{3}{2} p \ \psi_f i_{sq}$$
$$P_e = \frac{3}{2}\left(v_{sd} i_{sd} + v_{sq} i_{sq}\right) \tag{5}$$

2.3. Rotor shaft model

The rotor shaft of PMSG wind turbine is presented as a two-mass system and the motion equations are given in (Eq. (6)) where K is the stiffness of the shaft, θ is the shaft angle, J_g is the inertia of PMSG and J_T is the inertia of the wind turbine [44].

$$\begin{bmatrix} \dot{\omega}_T \\ \dot{\omega}_g \\ \dot{\theta} \end{bmatrix} = \begin{bmatrix} 0 & 0 & -\frac{K}{J_T} \\ 0 & 0 & \frac{K}{J_g} \\ 1 & -1 & 0 \end{bmatrix} \begin{bmatrix} \omega_T \\ \omega_g \\ \theta \end{bmatrix} + \begin{bmatrix} \frac{1}{J_T} \\ -\frac{1}{J_g} \\ 0 \end{bmatrix} \begin{bmatrix} T_w \\ T_e \end{bmatrix} \tag{6}$$

2.4. Grid model

The modeling of the grid side as shown in **Figure 5a** has two parts. The first part of modeling includes elements between the grid side convertor and the point of common coupling bus, which is known as a PCC bus. The first part dynamic model is based on the d-q frame of reference as shown in (Eq. (7)) [43, 44]; Where ω_s is the angular frequency of the grid, L_g and R_g are the inductance and resistance of the connecting transformer and power lines between the inverter and the PCC bus, respectively, v_{dpcc}, v_{qpcc}, $u_{di} v_{di}$, and v_{qi} u_{qi} represent the d- and q-axis components of the PCC voltage and grid side convertor, respectively, and i_{gd}, i_{gq} represent the d-q-axis components of the current flowing between the grid side convertor and the AC system. The expression of the active power is represented in (Eq. (8)) [43, 44].

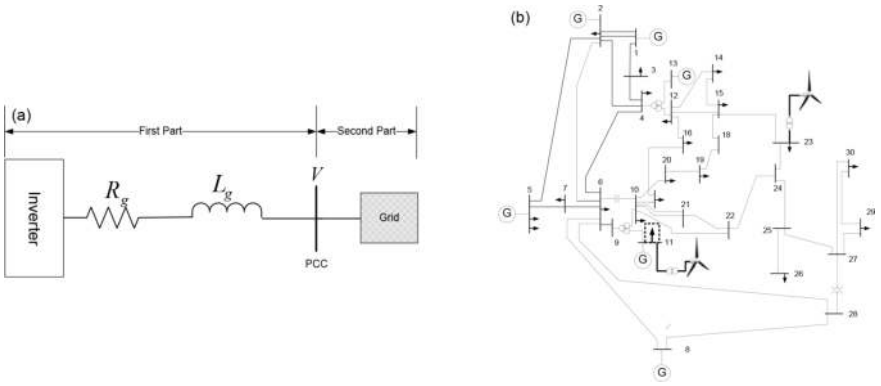

Figure 5. Grid side; (a) two parts of grid sides, (b) 30-bus system.

$$v_{di} = R_g i_{gd} + L_g \frac{d\, i_{gd}}{dt} - \omega_s L_g i_{gq} + v_{dpcc}$$
$$v_{qi} = R_g i_{gq} + L_g \frac{d\, i_{gq}}{dt} + \omega_s L_g i_{gd} + v_{qpcc} \tag{7}$$

$$P_g = \frac{3}{2}\left(v_{di}\ \ i_{gd} + v_{qi}\, i_{gq}\right) \tag{8}$$

The second part of the modeling is the grid model as shown in **Figure 5b** which is presented the IEEE 30 bus system using here as a sample of a 7-area system, where Area 5 and 7 are equipped with the PMSG wind turbine [45]. To simplify study the system stability, the power system loads have to be converted to the impedance as in (Eq. (9)), Therefore, the generators and loads impedances of the power system have to be include in the Y-bus. Also, the number of the buses in the original IEEE 30-bus have to be reduced to the number of generators [46]. The IEEE-30 bus system has 6 generators and two PMSG wind turbines. One of the PMSG wind turbines connected to the load bus and the another wind turbine connected to the PV bus. Therefore, The IEEE 30-bus reduced to the 7 bus or 7 areas system. In the area 5, the load was added to provide the disturbance of the system.

$$Y_L = \frac{P_L - J\, Q_L}{V_L^2} \tag{9}$$

The rotor variational dynamics of the synchronous generators, generator 1,2 to 7, in the reduced system are described in (Eq. (10)) [22], where D_j is the machine damping coefficient, $K_{sij} = V_i\, V_j\, Y_{ij} \sin\left(\theta_{ij} - \delta_i + \delta_j\right)$ are the synchronizing coefficient, P_w is the wind power, P_{mi} is the power that is from grid generators, ω_i is the speed of mass of the generators, and δ_i is the angular position of the mass. Area 7 connected to the load bus where $\omega_7 = K\, V_{dc}$ and K is a constant value. The unit of t is in s, ω in per-unit and $\omega_o = 314 \frac{r}{s}$.

$$\dot{\omega}_1 = \frac{\omega_0}{2\,H_1}\left(-D_1\,\omega_1 - \sum_{j=1}^{7} K_{s1}\,\delta_j + P_{m1} - P_{L1}\right), \qquad \dot{\delta}_1 = \omega_0\,\omega_1$$

$$\dot{\omega}_2 = \frac{\omega_0}{2\,H_2}\left(-D_2\,\omega_2 - \sum_{j=1}^{7} K_{s2}\,\delta_j + P_{m2} - P_{L2}\right), \qquad \dot{\delta}_2 = \omega_0\,\omega_2$$

$$\dot{\omega}_3 = \frac{\omega_0}{2\,H_3}\left(-D_3\,\omega_3 - \sum_{j=1}^{7} K_{s3}\,\delta_j + P_{m3} - P_{L3}\right), \qquad \dot{\delta}_3 = \omega_0\,\omega_3$$

$$\dot{\omega}_4 = \frac{\omega_0}{2\,H_4}\left(-D_4\,\omega_4 - \sum_{j=1}^{7} K_{s4}\,\delta_j + P_{m4} - P_{L4}\right), \qquad \dot{\delta}_4 = \omega_0\,\omega_4$$

$$\dot{\omega}_5 = \frac{\omega_0}{2\,H_5}\left(-D_5\,\omega_5 - \sum_{j=1}^{7} K_{s5}\,\delta_j + P_{m5} - P_{L5} + P_w\right), \qquad \dot{\delta}_5 = \omega_0\,\omega_5$$

$$\dot{\omega}_6 = \frac{\omega_0}{2\,H_6}\left(-D_6\,\omega_6 - \sum_{j=1}^{7} K_{s6}\,\delta_j + P_{m6} - P_{L6}\right), \qquad \dot{\delta}_6 = \omega_0\,\omega_6$$

$$\dot{\omega}_7 = \frac{\omega_0}{2\,H_7}\left(-D_7\,\omega_7 - \sum_{j=1}^{7} K_{s7}\,\delta_j - P_{L7} + P_w\right), \qquad \dot{\delta}_7 = \omega_0\,\omega_7 \tag{10}$$

2.5. DC-link model

The dc-link capacitor as shown in the **Figure 2** is connected between the generator and grid converter sides. The energy stored in the capacitor C is given by $E_{dc} = \frac{1}{2} C\,V_{dc}^2$, where V_{dc} is a dc-link voltage, and it depends on the difference between the generator power P_e and grid power P_g if the losses of both converters are considered very small as [8, 44].

$$C\,V_{dc}\,\frac{dV_{dc}}{dt} = P_e - P_g \tag{11}$$

To sending power from the wind turbine to the grid, the variation of the dc voltage has to be small or equal to zero which means the sending power P_e and receiving power P_g are equal.

3. Small signal stability

In this study, the small signal stability of the PMSG wind turbine connected to the power grid is going to be discuss at a particular operating point. The small signal stability is ability of the system to maintain stable during any small disturbance occurrence. In the power system,

disturbances with small magnitude are very common and can occur due to change in the generation power, power load. To study the small signal stability, the nonlinear system modeling such as wind turbine and dc-link modes has to be linearized to derive the state space matrix for the entire system by using the component connection techniques [22].

3.1. Linearization of the wind torque model

As in (Eq. (3)), the torque of the wind turbine is a function of the $C_p(\lambda, \beta)$; therefore, it has to be linearized respect to the wind speed, rotational speed, and blade pitch angle at operating point as [44].

$$\Delta T_w = K_w\, \Delta \mathrm{V_w} + K_T\, \Delta \omega_\mathrm{T} + K_\beta\, \Delta\beta \tag{12}$$

where

$$K_w = \frac{\partial T_w}{\partial V_w} = \frac{\sigma\, \pi R^2 V_{wo}^2}{2\, \omega_{\mathrm{To}}} \left[3\, C_p(\lambda_o, \beta_o) - \lambda_o\, \frac{\partial C_p(\lambda, \beta_o)}{\partial \lambda}\right]_{op}$$

$$K_T = \frac{\partial T_w}{\partial \omega_\mathrm{T}} = \frac{\sigma\, \pi R^2 V_{wo}^3}{2\, \omega_{\mathrm{To}}^2} \left[-C_p(\lambda_o, \beta_o) + \lambda_o\, \frac{\partial C_p(\lambda, \beta_o)}{\partial \lambda}\right]_{op}$$

$$K_\beta = \frac{\partial T_w}{\partial \beta} = \frac{\sigma\, \pi R^2 V_{wo}^3}{2\, \omega_{\mathrm{To}}}\, \frac{\partial C_p(\lambda_o, \beta)}{\partial \beta}$$

3.2. Linearization of a DC-link model

After substituting the sending and receiving power in to (Eq. (11)), the linearization of the d-link can be presented as

$$\begin{aligned}\Delta \dot{V}_{dc} = {} & \frac{3V_{sd}}{2CV_{dc}}\, \Delta i_{sd} + \frac{3I_{sd}}{2CV_{dc}}\, \Delta v_{sd} + \frac{3I_{sd}V_{sd}}{2CV_{dc}^2}\, \Delta v_{dc} + \frac{3V_{sq}}{2CV_{dc}}\, \Delta i_{sq} + \frac{3I_{sq}}{2CV_{dc}}\, \Delta v_{sq} + \frac{3I_{sq}V_{sq}}{2CV_{dc}^2}\, \Delta v_{dc} - \\ = {} & \frac{3V_{di}}{2CV_{dc}}\, \Delta i_{gd} - \frac{3I_{gd}}{2CV_{dc}}\, \Delta v_{di} + \frac{3I_{gd}V_{di}}{2CV_{dc}^2}\, \Delta v_{dc} - \frac{3V_{qi}}{2CV_{dc}}\, \Delta i_{gq} + \frac{3I_{gq}}{2CV_{dc}}\, \Delta v_{qi} + \frac{3I_{gq}V_{qi}}{2CV_{dc}^2}\, \Delta v_{dc}\end{aligned} \tag{13}$$

where Δv_{dc} is a variation of a DC voltage.

After describing the system modeling and its linearization, the interconnection method between the system modeling with its control has to be apply to create the state space equation for the entire system to study the system stability. **Figure 6(a–e)** shows the generator and grid sides with their controls. The way how to connect all the system models and controls together will be presented by getting the state variable of the entire system modeling with their controls as follows [47].

$$\begin{aligned}\dot{X} &= A\, X + B\, U \\ Y &= C\, X + D\, U\end{aligned} \tag{14}$$

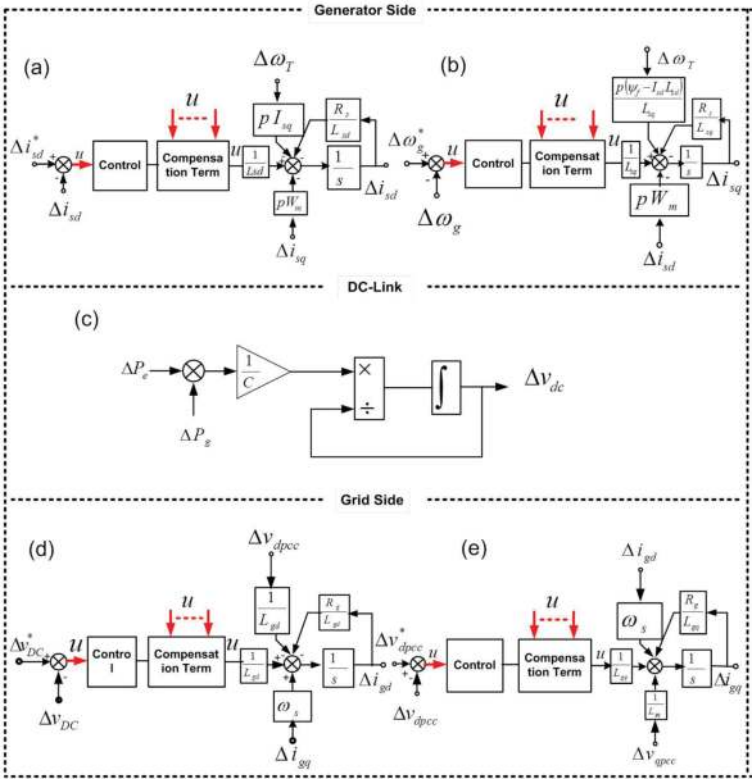

Figure 6. Connection of the PMSG models with its controls.

The system modeling of the PMSG with its controls as in **Figure 6** has to be connected together to get the state space equation. The interconnection matrix which connect the PMSG wind turbine models together with their controls is as [47].

$$U = E\,Y + F\,U^{*} \tag{15}$$

Matrix E is the states input and control inputs, u, as described in **Figure 6** while matrix F represents the reference input of the controllers. By substituting the output of (Eq. (14)) to (Eq. (15)), the input of the system will be as

$$U = (1 - ED)^{-1}\,E\,C\,X + (1 - ED)^{-1}\;\;F\,U^{*} \tag{16}$$

By substituting the input U in (Eq. (16)) into the (Eq. (14)), the (Eq. (14)) can be represented as [47].

$$\begin{aligned} \dot{X} &= \widehat{A}\,X + \widehat{B}\,U^{*} \\ Y &= \widehat{C}\,X + \widehat{D}\,U^{*} \end{aligned} \tag{17}$$

where X is a state variables of the whole system and its controls, U is an input control, Y is an output of the system, $\widehat{A} = A + B\,(1 - ED)^{-1}\,EC$ is a state matrix for the whole system and its

control, $\widehat{B} = B\,(1 - ED)^{-1}\,F$ is the input system matrix after connecting with its control, $\widehat{C} = C + D\,(1 - ED)^{-1}\,EC$ is the output matrix of whole system, and $\widehat{D} = D\,(1 - ED)^{-1}\,F$ is the direct transition matrix of the entire system. By getting the state matrixes of the entire system the eigenvalue sensitivity method can be study. The original system of PMSG wind turbine with its control in **Figure 2** is of 15th order which is presented as $[\Delta i_{sd}, \Delta i_{sq}, \Delta\omega_T, \Delta\omega_g, \Delta\theta, \Delta v_{dc}, \Delta i_{gd}, \Delta i_{gq}, \Delta x_1, \Delta x_2, \Delta x_3, \Delta x_4, \Delta x_5, \Delta x_6, \Delta\theta_{pll}]$ corresponding to the d-current of PMSG, q-current of PMSG, mechanical speed of the wind turbine PM generator speed, rotor shaft angle, dc voltage, d-current of grid, q-current of grid, PMSG speed control, PMSG speed control, dc-voltage control, q-current of grid control, PCC voltage control, PLL control and PLL angle, respectively; where; this original system can be reduced by ignoring the fast dynamic mode into 5th order as in **Figure 7**. As a result, the slow dynamic modes of the system are the Δi_{sq}, $\Delta\omega_T$, $\Delta\omega_g$, $\Delta\theta$ and Δx. With reference to **Figure 2**, the PI speed controller determines the q-axis stator voltage. The state equation of this controller is given by (Eq. (18)) and its output by (Eq. (19)). According to the same figure, the v_{sd} determined such that i_{sd} is zero for unity power

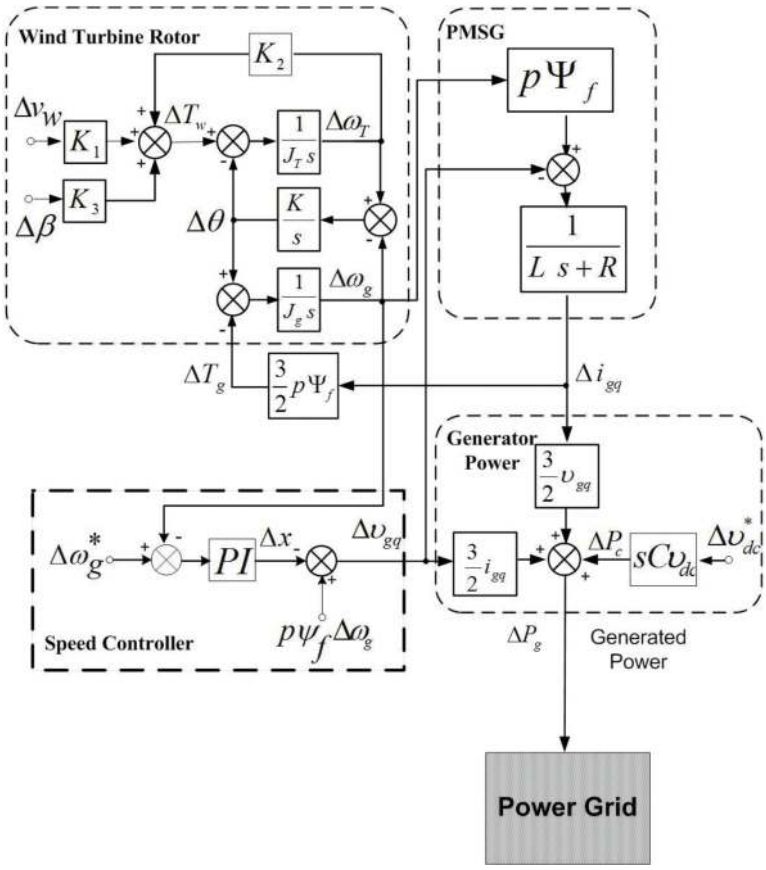

Figure 7. Reduced system.

factor operation. Because of the response of this loop is considerably faster than the inter-area dynamics of interest, the d-axis of (Eq.(4)) can be eliminated from the motor state equation by assuming that $\Delta i_{sd} = \Delta i_{\cdot sd} = 0$. Therefore, using (Eq. (19)) into q-axis of (Eq. (4)) and the previous condition, one obtains (Eq. (20)) that describes the simplified q-axis dynamics [44].

$$\Delta \dot{x} = \Delta \omega_g^* - \Delta \omega_g \tag{18}$$

$$\Delta v_{gq} = K_p \left(\Delta \omega_g^* - \Delta \omega_g \right) + K_i \, \Delta x + p \, \psi_f \, \Delta \omega_g \tag{19}$$

$$\Delta i_{gq} = -\frac{R}{L_{sq}} \, \Delta v_{gq} + \frac{K_p}{L_{sq}} \, \Delta \omega_g - \frac{K_i}{L_{sq}} \, \Delta x - \frac{K_p}{L_{sq}} \, \Delta \omega_g^* \tag{20}$$

The reduced system equation is described in (Eq. (6)), (Eq. (18)), and (Eq. (20)), which can be written as [44].

$$\begin{bmatrix} \Delta \dot{\omega}_T \\ \Delta \dot{\omega}_g \\ \Delta \dot{\theta} \\ \Delta \dot{x} \\ \Delta \dot{i}_{sq} \end{bmatrix} = \begin{bmatrix} \frac{K_T}{J_T} & 0 & -\frac{K}{J_T} & 0 & 0 \\ 0 & 0 & \frac{K}{J_g} & 0 & -\frac{\frac{3}{2} \, p \, \psi_f}{J_g} \\ 1 & -1 & 0 & 0 & 0 \\ 0 & -1 & 0 & 0 & 0 \\ 0 & \frac{K_p}{L_{sq}} & 0 & -\frac{K_i}{L_{sq}} & -\frac{R_s}{L_{sq}} \end{bmatrix} \begin{bmatrix} \Delta \omega_T \\ \Delta \omega_g \\ \Delta \theta \\ \Delta x \\ \Delta i_{sq} \end{bmatrix} + \begin{bmatrix} \frac{K_w}{J_T} & \frac{K_\beta}{J_T} & 0 \\ 0 & 0 & 0 \\ 0 & 0 & 0 \\ 0 & 0 & 1 \\ 0 & 0 & -\frac{K_p}{L_{sq}} \end{bmatrix} \begin{bmatrix} \Delta v_w \\ \Delta \beta \\ \Delta \omega_g \end{bmatrix} \tag{21}$$

4. H_∞ control method with wind generation

Figure 8 shows the H-infinity feedback control from grid to the PMSG speed, dc-voltage, and blade pitch angle controls. The wind generators in Area 5 and Area 7 act as a power source in the dynamic equation to increase the system damping by using the local frequency of machine 5 and wind turbine in Area 7, in order to achieve power modulation proportional to the frequency deviation of the area, e.g. $\Delta P_w = D \, \Delta \omega_5$ and $\Delta P_w = D \, \Delta \omega_7$. From **Figure 8**, the input power to the grid ΔP_w can be presented as

$$\Delta P_w = \frac{3}{2} \, \rho \, \psi_f \left(i_{sq} \, \Delta \omega_g + \omega_g \, \Delta i_{sq} \right) - C \, V'_{dc} \, \Delta \dot{V_{dc}} \tag{22}$$

The feedback signal is the locally derived system frequency deviation, $\Delta\omega_5$ and $\Delta\omega_7$, and the control outputs are the variations of the blade pitch angle, $\Delta\beta$, the rotor speed reference, $\Delta\omega_g^*$, and the rate of change of the dc link voltage reference, $\Delta \dot{V}_{dc}$. To design the H-infinity control, the plant consisting of the wind generation and the power system is considered controllable and observable. The state representation of the plant including the disturbance is given by (Eq. (23)) [48].

http://dx.doi.org/10.5772/intechopen.74835

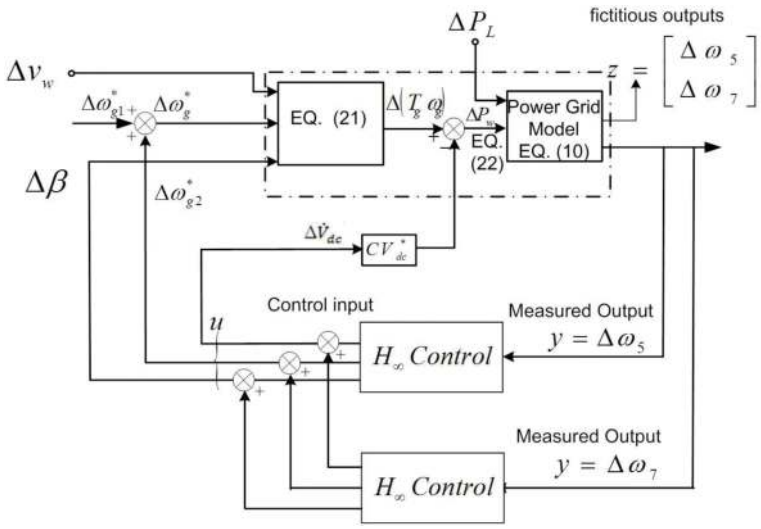

Figure 8. Power modulation control of the PMSG wind generator based on the H_∞ controller.

$$\begin{bmatrix} x \\ z \\ y \end{bmatrix} = \begin{bmatrix} A & B_d & B_u \\ C_1 & D_{11} & D_{12} \\ C & D_{21} & D_{22} \end{bmatrix} \begin{bmatrix} x \\ d \\ u \end{bmatrix} \tag{23}$$

where is the state vector, $z = [\Delta\omega_5, \Delta\omega_7]^T$ is the fictitious output, $y = [\Delta\omega_5, \Delta\omega_7]$ is the measurement vector, $u = \left[\Delta\beta, \Delta\omega_2^*, \Delta\dot{V}_{dc}\right]$ is the control input vector, and $d = [\Delta v_w, \Delta P_L]$ is the disturbance vector of the plant. A, B_d, B_u, C_1, D_{11}, D_{12}, C, D_{21} and D_{22} are constant matrices of appropriate size depending on the power system order. For simplicity it is assumed that there is no direct feedback through term, i.e. $D_{22} = 0$. The state representation of the H_∞ controller is given by (Eq. (24)) [48].

$$\begin{bmatrix} \dot{x} \\ u \end{bmatrix} = K \begin{bmatrix} x \\ y \end{bmatrix} \tag{24}$$

where $K = \begin{bmatrix} \widehat{A} & \widehat{B} \\ \widehat{C} & \widehat{D} \end{bmatrix}$ is the controller matrix and $\hat{x}$ is the controller state. The state representation of the closed-loop system is obtained by combining (23, 24); therefore:

$$\begin{bmatrix} \dot{x} \\ \dot{\hat{x}} \\ - \\ z \end{bmatrix} = \begin{bmatrix} A + B_u K C & 0 & - & B_d + B_u K D_{21} \\ 0 & K & - & 0 \\ - & - & - & - \\ C_1 + D_{12} K C & 0 & - & D_{11} + D_{12} K D_{21} \end{bmatrix} \begin{bmatrix} x \\ \hat{x} \\ - \\ d \end{bmatrix} = \begin{bmatrix} A_K & B_K \\ C_K & D_K \end{bmatrix} \begin{bmatrix} x_K \\ d \end{bmatrix} \tag{25}$$

The closed-loop transfer function, $\mathcal{F}(s)$, from d to z will be denoted as

$$f(s) = [D_{11} + D_{12}KD_{21}] + [C_1 + D_{12}KC \quad 0]\left(s\begin{bmatrix}1 & 0\\ 0 & 1\end{bmatrix} - \begin{bmatrix}A + B_uKC & 0\\ 0 & K\end{bmatrix}\right)^{-1}\begin{bmatrix}B_d + B_uKD_{21}\\ 0\end{bmatrix} \tag{26}$$

Matrices $\widehat{A},\ \widehat{B},\ \widehat{C},\ \widehat{D}$ are selected that the $f(s)$ is stable and the infinite norm, $\|f(s)\| < \gamma$ where, γ is a specified positive number.

5. Simulation studies

The IEEE 30-bus system as in **Figure 5(b)** was studied. The data for the lines, generators and loads are shown in [45]. Generator at bus 1 is the slack bus, in the simulations, and it is equipped with a governor for regulating frequency. The data of the wind generator on area 5 and area 7 are given in **Table 1**. Initially 50 wind generators were installed in each area, area 5 and area 7.

At the steady state generators 1–7 generate respectively 38, 43, 59, 5, 38, 13, and 77 MW. The initial wind velocity at the wind generator site is 11 m/s, and the wind generator generates an additional 77 MW of power. The power system dynamics are of the 14th order according to (Eq. (10)). The combined system including the dynamics of the wind generator from (Eq. (21)) is of the 19th order. The system and controller above was simulated in the time domain in MATLAB/SIMULINK. Two case studies were considered and the results are presented below.

Parameters	**Value**
Pole pairs	40
Rated power per generator	2 MVA
Generator rated voltage	575 V
Frequency	50 Hz
Stator resistance	0.0025 pu
Inductance in d-axis	0.43 pu
Inductance in q-axis	0.43 pu
Permanent magnet flux	1pu
PMSG inertia	2.5×10^5 kgm^2
Wind turbine inertia	3.7×10^6 kg m^2
DC link voltage	1500 V
DC-link capacitor per generator	60,000 μF

Table 1. Wind generator parameters [27].

http://dx.doi.org/10.5772/intechopen.74835

Case 1: Load change.

The load on Bus 5 changes from 50 to 60 MW at t = 1 s and the was operated at steady state. **Figure 9** shows the responses of the system with and without the feedback control from the wind generator. The result shows a power unbalance in the area 5 initiating and the net power exported by each area causes a large oscillations. As the system is adjusting to the new steady state, the exported power from the slack Bus 1 is increasing and that of Area 5 is decreasing by the same amount equal to the load change of 10 MW. From the figure the changing of the load power is absorbed by the infinite bus. Another Areas start oscillation when the load change and goes to the same operating point.

Figure 10(a) shows the response of the wind power resulting from the disturbance. The wind generator response is immediate providing approximately a peak variation of 5 MW power. The modulation power is created by the deviation of the dc link voltage, blade pitch angle, and generator speed shown in **Figure 10 (b–d)** respectively. The deviation of the dc link voltage of only 100 V or 6.6% is sufficient, and variation of the blade pitch angle is less than 0.1 degree and PMSG speed is very small.

Case 2: Wind speed change.

The system operates at the same steady state described above. At t = 1 s, the wind generator power increases from 77 to 100 MW when the wind velocity changes from 11 to 12 m/s.

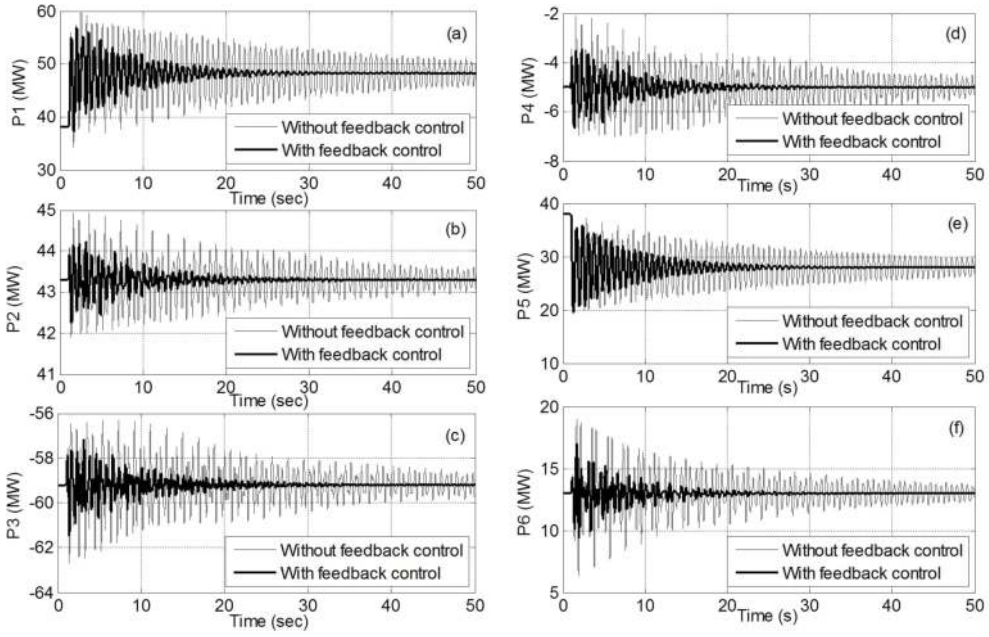

Figure 9. Case 1, load change: (a) net power of area 1; (b) net power of area 2; (c) net power of area 3, (d) net power of area 4; (e) net power of area 5; (f) net power of area 6.

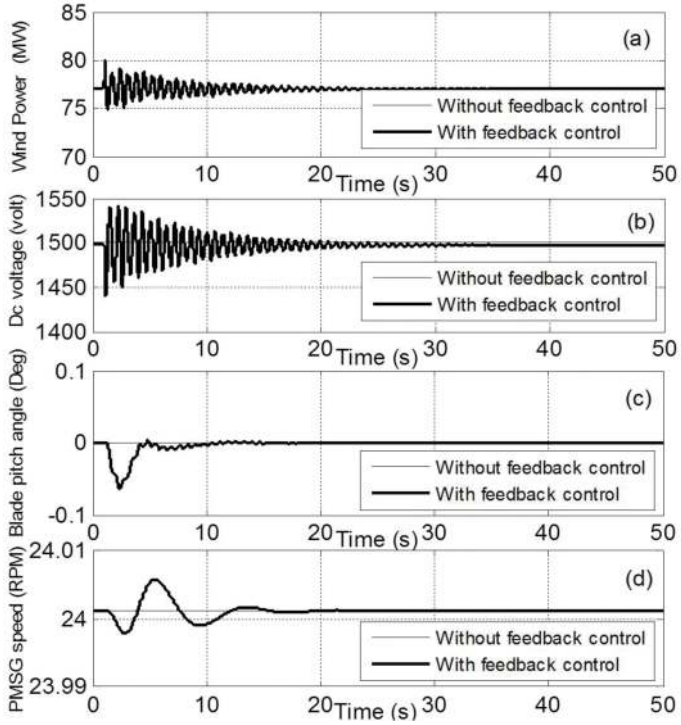

Figure 10. Load change: (a) wind power; (b) DC voltage response; (c) pitch angle response; (d) PMSG speed response.

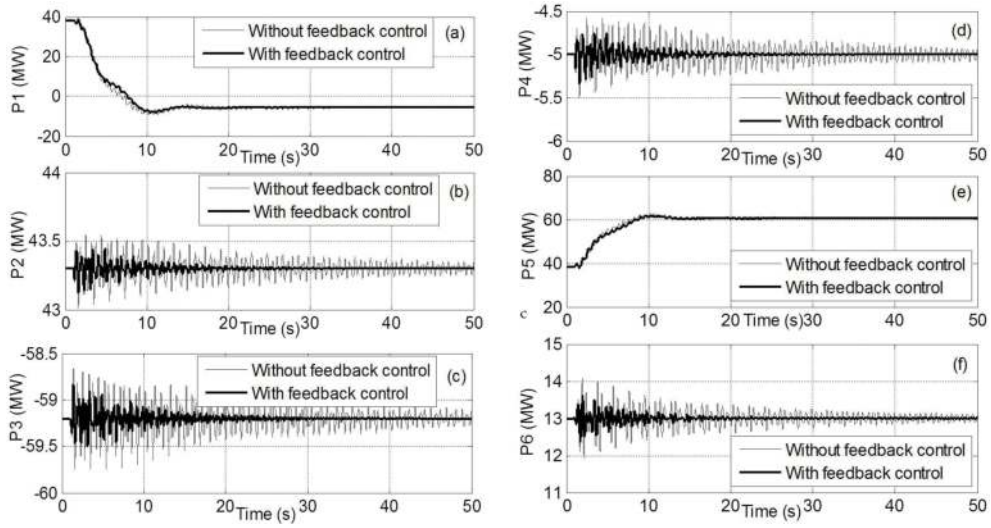

Figure 11. Case 1, load change: (a) net power of area 1; (b) net power of area 2; (c) net power of area 3. (d) Net power of area 4; (e) net power of area 5; (f) net power of area 6.

Therefore, the additional power injected into areas 5 and 7 initiate acceleration of the machines at areas 5 and 7 and, subsequently, similar response at the other machines. **Figure 11(a–f)** shows the net power with and without power modulation feedback when the wind speed changed from 11 to 12 m/s at t = 1 s. The event causes a power unbalance in the area served by area 5 and 7 initiating exhibiting large oscillations. As the system is adjusting to the new steady state, the exported power from the slack Bus 1 is decreasing and that of area 5 and area 7 are decreasing by the same amount equal to the wind power change by of 46 MW. The effectiveness of the wind power modulation by using H-infinity feedback control can be seen in **Figure 11(a–f)** comparing to the responses without power modulation. The oscillation damping has increased significantly and the system arrives at the steady state approximately 20s.

Figure 12 shows the responses of the system with and without the feedback control from the wind generator at t = 1 with changing of the wind speed from 11 to 12 m/s. The output of the wind generator power as in **Figure 12(a)** is smooth increasing to accelerate the PM-generator.

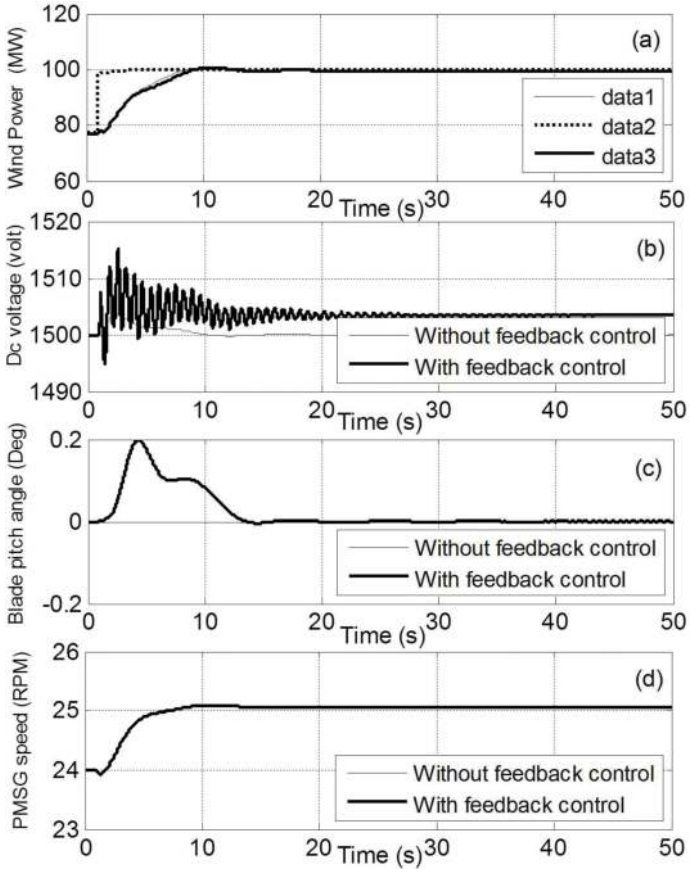

Figure 12. Wind speed change: (a) wind power; (b) DC voltage response; (c) pitch angle response; (d) PMSG speed response.

The oscillations in the dc link voltage are greater in the case where modulation feedback is used resulting partly in the stabilizing power modulation. The deviation of the dc link voltage of only 20 V or 1.3% is sufficient. The blade pitch angle, in **Figure 12(c)**, is activated only by the power modulation feedback and the variation of the blade pitch angle is less than 0.2°. The generator speed, in **Figure 12(d)**, immediately accelerates as a result of the increasing wind power input and its variation is very small.

6. Conclusion

The power modulation by using a PMSG wind turbine to damp the power oscillation in a multi-area power system is studied. H-infinity control is applied as a feedback control; where, the input is the variation of the local grid generator speed and the output feedback to the dc-voltage, blade pitch angle and PMSG speed controls. The high-order dynamic model of the wind generator system is reduced to simplify the analysis. The PMSG wind turbine connected to the IEEE 30 bus in different areas such as area 5 and 7. The results showed the effectiveness of the wind generator in significantly increasing damping. The dc link voltage modulation provides more damping to the grid power oscillations as it compares to the PMSG speed and rotor blade pitch angle modulations. The MATLAB/Simulink is used to design the controller and validate the results.

Author details

Emad M. Elhaji[1,2]

Address all correspondence to: emadelhaji@siu.edu

1 Misurata University, Misurata, Libya

2 Sothern Illinois University, Carbondale, USA

References

[1] Forsberg CW. Sustainability by combining nuclear, fossil and renewable energy sources. Progress in Nuclear Energy. 2009;**51**:192-200

[2] Matas J, Castilla M, Guerrero JM, Garcia De Vicuna L, Miret J. Feedback linearization of direct-drive synchronous wind-turbines via a sliding mode approach. Power Electronics, IEEE Transactions on, May 2008;**23**(3):1093-1103

[3] Wind Power Today and Tomorrow - NREL - U.S. Department of Energy — Energy Efficiency and Renewable Energy By the National Renewable Energy Laboratory, a DOE National laboratory DOE/GO-102004-1894 March 2004

[4] Global Wind Report Annual Market Update. Gwec.net. Retrieved 2017–05-5

[5] Technology Roadmap Wind energy – International Energy Agency, 2013

[6] González-Longatt FM, Wall P, Terzija V. A simplified model for dynamic behavior of permanent magnet synchronous generator for direct drive wind turbines. In: 2011 IEEE Trondheim PowerTech. Trondheim; 2011. pp. 1-7

[7] Muljadi M, Singh M, Gevorgian V. Fixed-Speed and Variable-Slip Wind Turbines Providing Spinning Reserves to the Grid. National Renewable Energy Laboratory (NREL), Tech. Rep; July 2013

[8] Devaraj D, Jeevajyothi R. Impact of fixed and variable speed wind turbine systems on power system voltage stability enhancement. Renewable Power Generation (RPG 2011), IET Conference on. 2011:1-9

[9] Carlin P, Laxson A and Muljadi E. The history and state of the art of variables speed wind turbine technology. National Renewable Energy Lab., Golden, CO, Tech. Rep. NREL/TP-500-28 607; 2001

[10] Cao W, Xie Y, Zheng T. Wind Turbine Generator Technologies. InTechOpen; 2012

[11] Ali HR. "The dynamic performance of grid-connected fixed-speed wind turbine generator," 2014 6th International Conference on Information Technology and Electrical Engineering (ICITEE), Yogyakarta, 2014, pp. 1-5

[12] Camm EH et al., "Characteristics of wind turbine generators for wind power plants," 2009 IEEE Power & Energy Society General Meeting, Calgary, AB, 2009, pp. 1-5

[13] Fletcher J, Yang J. Introduction to doubly-fed induction generator for wind power applications. In: Nathwani J, Ng AW, editors. Paths to Sustainable Energy. New York, NY, USA: InTech; 2010. pp. 259-278

[14] Morimoto S, Nakayama H, Sanada M, Takeda Y. Sensorless output maximization control for variable-speed wind generation system using IPMSG. IEEE Transactions on Industry Applications. Jan.-Feb. 2005;**41**(1):60-67

[15] Teodorescu R, Liserre M, Rodríguez P. Grid converter structures for wind turbine systems. In: Grid Converters for Photovoltaic and Wind Power Systems. Chichester, UK: John Wiley & Sons, Ltd; 2011. DOI: 10.1002/9780470667057.ch6

[16] Hoffmann R. A comparison of control concepts for wind turbines in terms of energy capture. In: D17 Darmstädter Dissertation. Germany: Department of Power Electronics and Control of Drives, Darmstadt; 2002. p. 134

[17] Tiwari Ramji, Sanjeevikumar P, Ramesh Babu N. "Co-ordinated control strategies for permanent magnet synchronous generator based wind energy conversion system", Energies Journal, MDPI AG Publications, Switzerland, 28 Sept. 2017;**10**(1493):1-17

[18] Courseware Sample: Principles of Doubly-Fed Induction Generators (DFIG), Festo Didactic Ltee/Ltd, 2011

[19] Hanselman DC. Brushless Permanent Magnet Motor Design. USA: McGraw-Hill; 1994

[20] Akin B, Bhardwaj M. "Sensored Field Oriented Control of 3-Phase Induction Motors", Copyright © 2013, Texas Instruments Incorporated, SPRABP8–July; 2013

[21] Liang J and Whitby B. "Field oriented control of a permanent magnet synchronous generator for use in a variable speed tidal stream turbine," Universities' Power Engineering Conference (UPEC), Proceedings of 2011 46th International, Soest, Germany, 2011, pp. 1-6

[22] Kundur P. Power System Stability and Control. USA: McGraw Hill; 1994

[23] Klein M, Rogers GJ, Kundur P. A fundamental study of inter-area oscillations in power systems. In IEEE Transactions on Power Systems. Aug 1991;**6**(3):914-921

[24] Hsu YY, Shyue SW, Su CC. Low frequency oscillations in longitudinal power systems: Experience with dynamic stability of Taiwan power system. In IEEE Transactions on Power Systems. Feb. 1987;**2**(1):92-98

[25] Kim M-K. Optimal control and operation strategy for wind turbines contributing to grid primary frequency regulation. Applied Sciences. 2017;**7**:927

[26] Fatu M, Tutelea L, Boldea I and Teodorescu R. Novel motion sensorless control of stand alone permanent magnet synchronous generator (PMSG): Harmonics and negative sequence voltage compensation under nonlinear load. 2007 European Conference on Power Electronics and Applications, Aalborg, 2007, pp. 1-10

[27] Li S, Haskew TA, Swatloski RP, Gathings W. Optimal and Direct-Current vector control of direct-driven PMSG wind turbines. Power Electronics, IEEE Transactions on. May 2012; **27**(5):2325-2337

[28] Ganesh A, Dahiya R, Singh GK. A novel STATCOM wide area feedback controller for improving stability in multimachine system. In: Power Systems, Energy, Environment. 2014

[29] Tsourakis G, Nomikos BM, Vournas CD. Contribution of doubly fed wind generators to oscillation damping. IEEE Transactions on Energy Conversion. Sep. 2009;**24**(3):783-791

[30] Margaris ID, Papathanassiou SA, Hatziargyriou ND, Hansen AD, Sorensen P. Frequency control in autonomous power systems with high wind power penetration. In IEEE Transactions on Sustainable Energy. April 2012;**3**(2):189-199

[31] Sun YZ, Zhang ZS, Li GJ and Lin J. "Review on frequency control of power systems with wind power penetration," 2010 International Conference on Power System Technology, Hangzhou, 2010, pp. 1-8

[32] Dengying, Zhoujie. LPV H-infinity controller Design for a Wind Power Generator. 2008 IEEE Conference on Robotics, Automation and Mechatronics, Chengdu, 2008, pp. 873-878

[33] Howlader A, Urasaki N, Yona A, Senjyu T, Saber A. Design and Implement a Digital H∞ Robust Controller for a MW-Class PMSG-Based Grid-Interactive Wind Energy Conversion System. Energies. June 2013:pp. 2084-2109

[34] Muhando BE, Wies RW. Nonlinear H_∞ constrained feedback control for grid-interactive WECS under high stochasticity. In IEEE Transactoons Energy Conversion. Dec. 2011;**26**(4): 1000-1009

[35] Muhando EB, Senjyu T, Uehara A, Funabashi T. Gain-scheduled H_∞ control for WECS via LMI techniques and parametrically dependent feedback part I: Model development fundamentals. In IEEE Transactions on Industrial Electronics. Jan. 2011;**58**(1):48-56

[36] Geng H, Dewei X. Stability analysis and improvements for variable-speed multipole permanent magnet synchronous generator-based wind energy conversion system. Sustainable Energy, IEEE Transactions on. Oct. 2011;**2**(4):459-467

[37] Alaboudy A, Daoud A, Desouky S, Salem A. Converter controls and flickers study of PMSG-based grid connected wind turbines. Ain Shams Engineering Journal. March 2013; **4**(1):75-91

[38] Haque Md E, Negnevitsky M, Muttaqi KM. A novel control strategy for a variable-speed wind turbine with a permanent-magnet synchronous generator. Industry Applications, IEEE Transactions on. Jan.-feb. 2010;**46**(1):331-339

[39] Belhadj J, Roboam X. Investigation of different methods to control a small variable-speed wind turbine with PMSM drives. Journal of Energy Resources Technology. 2007;**129**(3): 200-213

[40] Geng H et al. Active damping for PMSG-based WECS with DC-link current estimation. Industrial Electronics, IEEE Transactions on. 2011;**58**(4):1110-1119

[41] Zhang Z, Hackl C, Kennel R. Two direct torque and power control methods for back-to-back power converter PMSG wind turbine systems. presented at the Int. Power Electronics Motion Control Conf. Hefei, China. May 2016

[42] Rosyadi M, Muyeen SM, Takahashi R, Tamura J. Transient stability enhancement of variable speed permanent magnet wind generator using adaptive PI-fuzzy controller. PowerTech, 2011 IEEE Trondheim, 1,6, 19-23 June 2011

[43] Elhaji EM, Hatziadoniu CJ. Damping tie-line power oscillations by modulation feedback of wind generators. Electric Power Systems Research. 2016

[44] Elhaji EM, Hatziadoniu CJ. Interarea oscillation damping using H-infinity control for the permanent magnet wind generator. Electric Power Systems Research. 2017

[45] Power system test cases archive, available on www.ee.wasinton.edu/research/pstca

[46] Anderson, Paul M, and Aziz A. Fouad. Power system control and stability. John Wiley & Sons, 2008.ower system book for 9-bus system

[47] Ortega R, Garcia-Canseco E. Interconnection and damping assignment passivity-based control: A survey. European Journal of Control. 2004;**10**:432-450

[48] Burke JV et al. HIFOO-a MATLAB package for fixed-order controller design and H∞ optimization. In: Fifth IFAC Symposium on Robust Control Design, Toulouse. 2006